International Journal of the Physical Sciences Vol. 5(7), pp. 1200-1211, July 2010
Available online at http://www.academicjournals.org/IJPS
ISSN 1992 - 1950 ©2010 Academic Journals

Full Length Research Paper

A new algorithm for the design of uniform and nonuniform arrays of coupled optical waveguides

T. A. Ramadan

Department of Physics, Faculty of Science, Kuwait University, P. O. Box 5969, Safat 13060, Kuwait. Department of Electronics and Electrical Communication Engineering, Ain Shams University, Abbasia 11517, Cairo, Egypt. E-mail: tarek.ramadan@ku.edu.kw.

Accepted 10 June, 2010

An algorithm is proposed for the design of both uniform and nonuniform arrays of coupled waveguides. The algorithm identifies the array parameters which support different number of modes. It uses a general cutoff dispersion function which eliminates the need to solve complex dispersion equations. Numerical examples are included to verify the utility of the proposed algorithm.

Key words: Coupled waveguide arrays, numerical analysis, optical waveguides, waveguide theory.

INTRODUCTION

Coupled waveguide arrays are basic elements of photonic integrated circuits, e.g. in (Raburn et al., 2000; Lee et al., 2004; Hammer et al., 2004; Dross et al., 2005; Xia et al., 2005; Menon et al., 2005; Passaro and Masanovic, 2006; Saeedkia and Safavi-Naeini, 2007; Belabas et al., 2009). They may couple between single-mode or multimode waveguides (Hardy et al., 1986; Shama et al., 1989). The coupling to multimode guides may be used in power splitters (Hardy et al., 1988), multiplexers and switches (Ramadan et al., 2000), or optical filters (Liu and Magnusson, 2002). The waveguides in these arrays may have differences in their thickness, refractive index, or separation. These differences may stem from design requirements such as asynchronicity of grating couplers (Marcuse, 1987) or phase change to achieve wavelength routing in straight arrayed waveguide gratings (Kawakita et al., 2004). It may result from coupling between different multilayer guides in the vertical direction (Rajarajan et al., 2003; Xia et al., 2005; Menon et al., 2005) or changing the coupling constant in the lateral direction (Belabas et al., 2009). While these differences add degrees of freedom in the design of photonic devices, they greatly complicate this design. Specifically, in identifying the array parameters, which support different number of modes. These parameters cannot be identified by the standard coupled mode theory under strong coupling conditions. Their identification is a critical design step, which defines the feasible parameter space over which other modal and/or performance parameters are computed and optimized. For example, as in maximizing available laser power (Dross et al., 2005), fiber coupling efficiency (Buus et al., 1993; Xia et al., 2005; Menon et al., 2005) or photomixing in terahertz generators (Saeedkia and Safavi-Naeini, 2007), under a fixed number of unperturbed guided modes. In the absence of exact analytical design rules which identify these parameters, only approximate or numerical approaches may be used, e.g. in (Hardy and Streifer, 1986; Syms, 1987; Chiang, 1991; Zhao et al., 1992; Scarmozzino et al., 2000). These approaches may either add restrictions to the design parameters or consume considerable time of computations to identify them.

The purpose of this paper is to present a simple and general algorithm that identifies the design parameters of coupled arrays of one-dimensional waveguides which support an arbitrary number of modes. The algorithm applies to uniform and nonuniform arrays under weak and strong coupling conditions for both TE and TM polarizations. It starts with parameters supporting an initial number of modes of an array, which may represent the vertically coupled guiding layers of a photonic device, e.g. in (Buus et al., 1993; Raburn et al., 2000; Lee et al., 2004; Hammer et al., 2004; Dross et al., 2005; Xia et al., 2005; Menon et al., 2005; Passaro and Masanovic, 2006; Saeedkia and Safavi-Naeini, 2007). Then, it monitors the sign of a general cutoff dispersion function to search for,

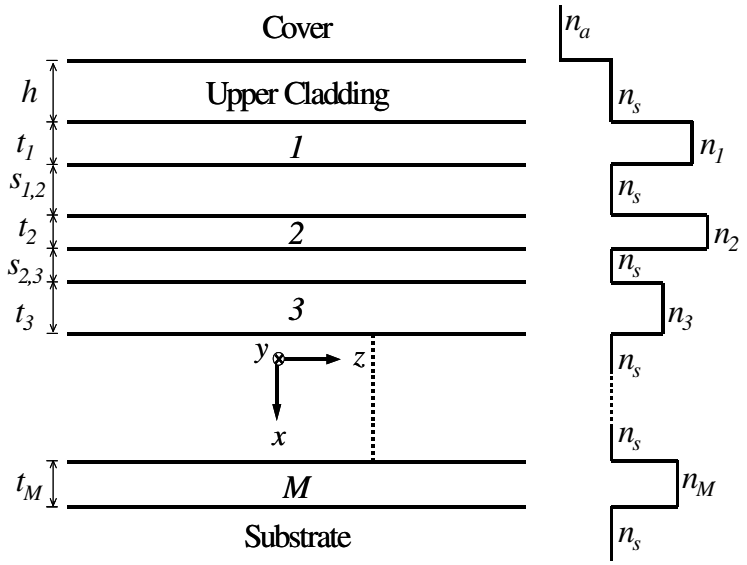

Figure 1. Schematic of a nonuniform array of *M* planar waveguides with the corresponding refractive index profile.

and tracks, the boundaries of the target parameter space that supports the required number of modes. This identification of array parameters involves no approximations. It may only be applied to the design of arrays of two-dimensional waveguides, e.g. in (Kawakita et al., 2004; Belabas et al., 2009), within the effective index approximation. The utility of the algorithm is demonstrated through general design examples which reflect the wide scope of the algorithm.

BACKGROUND THEORY

Differential mode counting

The number of guided modes supported by an array of coupled waveguides may change by changing any of their geometrical or refractive index parameters. The requirement that the effective refractive index, n_e, of each guided mode must cross-over the substrate refractive index, n_s, as the mode becomes guided or leaks into the substrate, implies a change in the sign of the corresponding dispersion function at cutoff (Ruschin et al., 1986). It allows computing the number of modes at any point of the parameter space in terms of the number of modes at another reference point by counting the number of changes in the sign of the cutoff dispersion function along an arbitrarily chosen path between these points. This count must exclude the changes in this sign due to poles of the dispersion function, which may crossover the cutoff point along that path. It is the basis of the search-and-track (SAT) algorithm presented in this paper.

Cutoff dispersion function

Consider the case of an array of *M* coupled waveguides impeded in a common substrate of refractive index, n_s (Figure 1). The m^{th} waveguide in this array has a thickness, t_m, refractive index, n_m, and is separated from the $m+1^{th}$ waveguide by $s_{m,m+1}$. The surface guide (m=1) has an upper cladding thickness, h, and a cover layer of refractive index, n_a.

The cutoff dispersion function of this array, C_M, is obtained by first deriving its dispersion function following the approach in (Chiang, 1992) and (Ramadan, 2008). Then, taking the limit of this function as the normalized propagation constant tends to zero. The results are given by the recurrence relation,

$$C_{m+1} = \rho_{m+1} C_m - \kappa_{m+1} C_{m-1} \qquad (1a)$$

with

$$C_2 = \hat{\rho}_2 C_1 - \hat{\kappa}_2 C_0 \,. \qquad (1b)$$

The recurrence index m in (1a) increases in steps from m = 2 to m = M - 1 in the direction of increasing x. The recurrence parameters are,

$$\rho_{m+1} = \cot(T_{m+1}) + \eta_{m,m+1} \cot(T_m) - \frac{S_{m,m+1}}{\varepsilon_{m+1}} \qquad (2a)$$

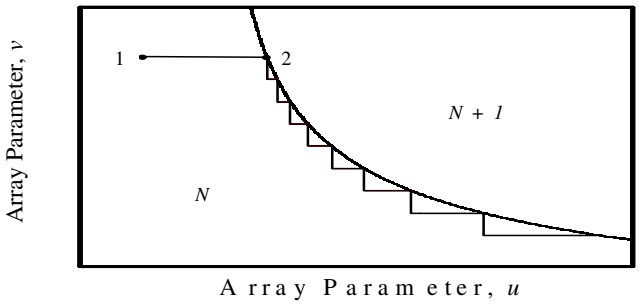

Figure 2. A horizontal search path extending from an initial guess point 1 (with N_o=N) to point 2, which represents the origin of the track, followed by a downward staircase track (solid) of the boundary (dashed) between two u-v parameter spaces supporting N and N+1 modes. Although not shown, vertical search paths as well as upward tracks may also be followed which results in four search and track possibilities.

$$\kappa_{m+1} = \eta_{m,m+1} \csc^2(T_m) \quad (2b)$$

$$\hat{\rho}_2 = \rho_2 + \frac{(\hat{\kappa}_2 - \kappa_2)}{C_1} \quad (2c)$$

and

$$\hat{\kappa}_2 = \frac{1+\sigma^2}{(1+\gamma_a\sigma)+(\sigma-\gamma_a)\cot(T_1)}\kappa_2 \quad (2d)$$

where

$$\eta_{m,m+1} = \frac{\varepsilon_m}{\varepsilon_{m+1}}\sqrt{\frac{\delta_{m+1}-1}{\delta_m-1}} \quad (2e)$$

$$\sigma = \frac{1}{\varepsilon_a\sqrt{a}} + \frac{H}{\varepsilon_1} \quad (2f)$$

and

$$\gamma_a = \frac{1-a\varepsilon_a^2}{2\varepsilon_a\sqrt{a}}. \quad (2g)$$

The cutoff dispersion functions, $C_1 = \cot(T_1) - \sigma$ and $C_0 = 1$. The normalized parameters, $T_m = (2\pi/\lambda_o)t_m\sqrt{n_m^2 - n_s^2}$, $S_{m,m+1} = (2\pi/\lambda_o)s_{m,m+1}\sqrt{n_{m+1}^2 - n_s^2}$, and $H = (2\pi/\lambda_o)h\sqrt{n_1^2 - n_s^2}$, where λ_o is the free-space wavelength. The asymmetry parameter, $a = (n_s^2 - n_a^2)/(n_1^2 - n_s^2)$, the waveguide refractive index parameter, $\delta_m = n_m^2/n_s^2$, and the polarization parameters, $\varepsilon_m = \varepsilon_a = 1$ for TE modes while $\varepsilon_m = \delta_m$ and $\varepsilon_a = n_1^2/n_a^2$ for TM modes.

The SAT algorithm uses (1) to compute the sign of C_M as it counts the number of modes of asymmetric arrays. For symmetric arrays $a \to 0$, $H \to \infty$, $\hat{\kappa}_2 \to \kappa_2$, $\hat{\rho}_2 \to \rho_2$, and $C_1 \to -\infty$, which lead to undefined values of C_M, whose signs cannot be determined. To avoid this problem, the sign of C_M is computed as the product of the sign of C_1 and the sign of the ratio of C_M to C_1. This ratio is well defined. It is computed using (1) by replacing C_1 with unity and C_0 with zero.

PROPOSED ALGORITHM

Search-and-track approach

Except for few special cases, the parameter space that supports a specific number of modes is closed. Here, a closed parameter space refers to a space which is bounded along any dimension except, perhaps, when one or more parameters along other dimensions are zeros. In order to identify the closed space of generalized array parameters u and v which support a specific number of guided modes, N, the proposed algorithm starts with an initial guess of a point that either belongs to this space (see point 1 in Figure 2) or to a space supporting N_o modes, which is different from N. This initial guess may either be obtained experimentally or

estimated using different physical and/or mathematical bounds.

After choosing the initial guess point (IGP), the algorithm searches for a point on the space boundaries. For example, point 2 at the boundary between the spaces supporting *N* and *N*+ 1 mode in Figure 2. It does so by moving along a single dimension in the horizontal (or the vertical) direction of the *u*-*v* space in infinitesimally small steps starting from the IGP, keeping the other space dimension unchanged. In moving along either of the horizontal or vertical search paths, it monitors the sign of C_M. Any unwanted sign changes due to function poles crossing the cutoff point must be filtered out following a rule which is given below. Once the number of sign changes exceeds the absolute difference between *N* and N_o, the motion along the horizontal (or vertical) dimension stops and the preceding point along the search path represents a point on the boundary that encloses the target space, which supports the required number of modes, *N*. The flow chart in Figure 3 provides detailed description of the search loop.

The boundary point 2, which is allocated by the search loop, is the origin of a staircase path that tracks that boundary as shown in Figure 2.

It is created by a step decrease (or increase) in the vertical (or horizontal) parameter of the *u*-*v* space starting from this origin point, followed by a search for a new boundary point along the horizontal (or vertical) search dimension of the *u*-*v* space. This step-and-search process continues until sufficient points are allocated to reconstruct the space boundary within a predefined computational window. It requires *a priori* knowledge of the shape of the boundary to determine the directions of increasing or decreasing *u* and *v* along the track. These directions are governed by a general rule, which is described below. The flow chart of Figure 3 provides detailed description of the staircase tracking loop.

Tracking rules

In order to reconstruct the boundaries of a specific parameter space using the SAT algorithm, the tracking directions of the *u* and *v* parameters along these boundaries must be known. As a preliminary step towards developing a tracking rule which specifies these directions, we may classify array parameters into two types depending on whether their increase may add modes to, or subtract modes from, the array. Next, the number of modes supported by the array is expressed as a two dimensional function $N(u,v)$ in the *u*-*v* space. The dependence of *N* on other array parameters is suppressed for simplicity. Let $Y(u,v)$ be a randomly selected continuous differentiable function associated with *N*, which satisfies the relation, $\lfloor Y \rfloor = N$. The value of Y at the upper or lower boundary of the space supporting *N* modes is denoted by Y_B. In the vicinity of this boundary, $Y = Y_B + \Delta Y$, where ΔY represents a first-order perturbation from Y_B. This perturbation may be expanded by the first-order terms of a Taylor series, $\Delta Y = (\partial Y/\partial u)_B \Delta u + (\partial Y/\partial v)_B \Delta v$, around the boundary. For all functions *Y*, which satisfy $\lfloor Y \rfloor = N$, their derivatives in this expansion must be positive for mode-adding parameters and negative for mode-subtracting parameters. If this is not the case, then it would contradict the definition of these derivatives which are computed at the boundaries of the space where *u* and *v* have their extreme values (minima (maxima) for mode-subtracting parameters and maxima (minima) for mode-adding parameters at the upper (lower) boundary). The relation between Δu and Δv at the boundary (upper or lower) is obtained by setting $\Delta Y = 0$ in the Taylor expansion. It gives,

$$\Delta v = -(\partial Y/\partial u)_B / (\partial Y/\partial v)_B \, \Delta u \qquad (3)$$

According to (3), Δu and Δv must have opposite (similar) signs whenever $(\partial Y/\partial u)_B$ and $(\partial Y/\partial v)_B$ have similar (opposite) signs. This result leads to a simple tracking rule, which states that: two array parameters of the same type must have opposite tracking directions (if one decreases, then the other increases and vice versa) while those of different types must have the same tracking direction (both increase or decrease) along the boundaries of the parameter space supporting a specific number of modes. For example, the increase in either the thickness of waveguides or their separation in an array never decreases the number of guided modes. It either increases it or keeps it constant. Therefore, t_m and $s_{m,m+1}$ must have opposite tracking directions along the boundaries of the t_m-$s_{m,m+1}$ space. Inspection of the design parameters of coupled waveguide arrays concludes that, except for the substrate refractive index, n_s, all other parameters (including t_m, $s_{m,m+1}$, n_m, *h*, and n_a) are mode-adding parameters. Note that the cover refractive index is constrained by $n_a \le n_s$. Since the free-space wavelength is a mode-subtracting parameter, normalization of any of the mode-adding parameters by λ_o does not change their type.

Filtering out sign changes due to poles

There are two groups of poles of the dispersion function of the coupled waveguide array (Appendix A). One group never crosses the cutoff point with the change in any array parameter. The other group crosses this point whenever the normalized thickness, T_m, of any waveguide crosses $q\pi$ between two successive points along a search path, where *q* is a positive integer. Each crossing of a pole of this group results in a change in the sign of C_M (Appendix B). Thus, to filter out sign changes due to poles, it is sufficient to flip the sign of C_M at each crossing of a pole during the search loop, as shown in the flow chart of Figure 3. If these sign changes are not filtered out, they result in a premature termination of the search path and faulty locations of the boundary points of the parameter space. The utility of this rule is verified by the application examples given below.

APPLICATIONS

Modal maps

In this section, the SAT algorithm identifies waveguide array parameters, which support different number of TE and TM modes. It starts by choosing an IGP, which belongs to the space supporting the minimum number of modes. The advantage of starting with this number is that the selection of the IGP reduces to the selection of the smallest possible *u* and *v* coordinates. Recall that all array parameters (except n_s) are mode-adding parameters. Alternatively, the IGP may be chosen using already known solutions for specific points in the *u*-*v* space (see below). Next, the algorithm allocates the upper boundary of the space, which supports the initial number of modes, as explained above. Then, the computations follow a sequential approach in allocating the boundaries of the subsequent

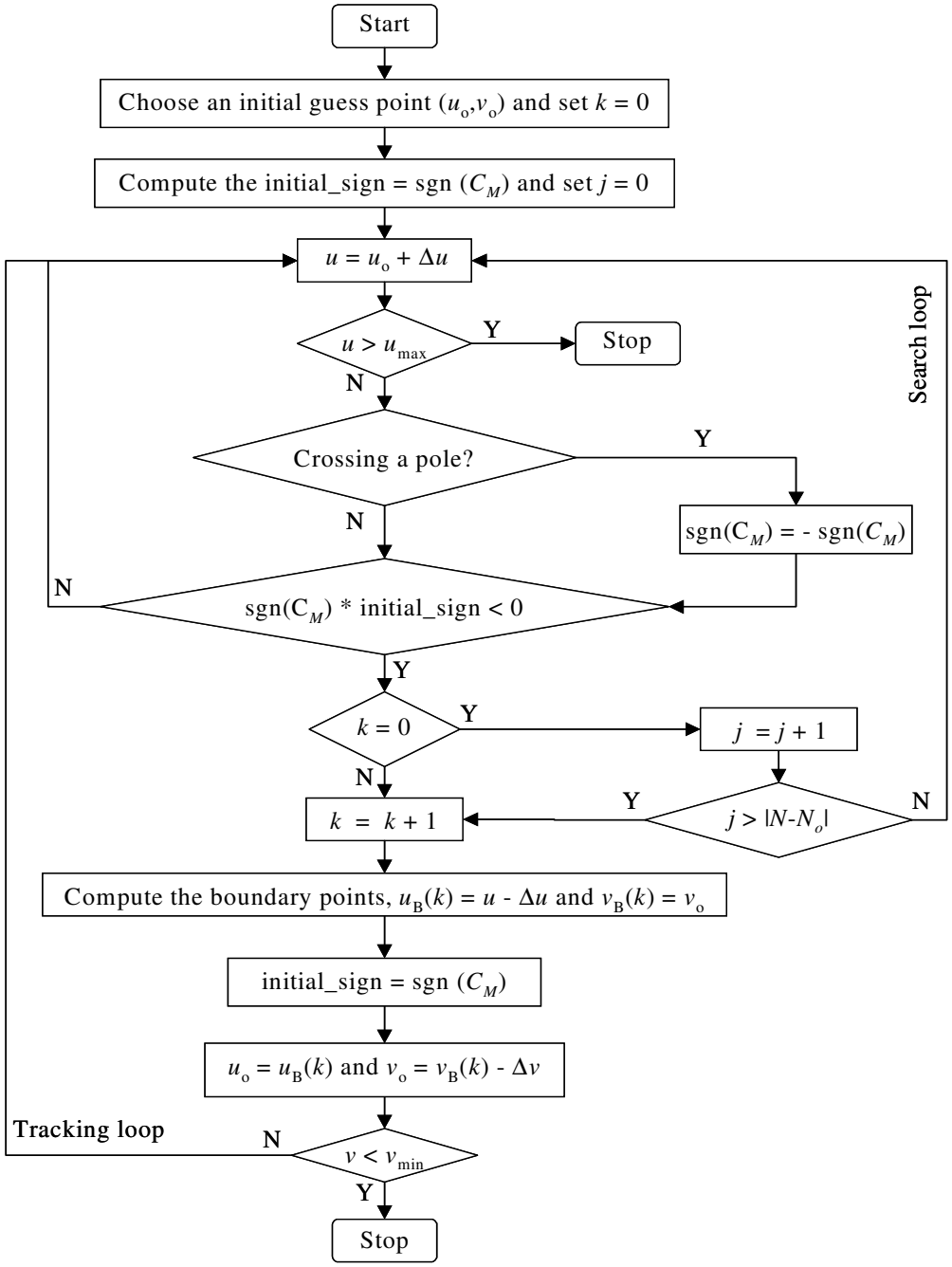

Figure 3. A flow chart description of a horizontal-search and downward-track algorithm. It assumes that *u* and *v* have opposite tracking directions. The index *j* counts the number of sign changes along the search path between points 1 and 2 of Figure 2. The index *k* counts the boundary points. The vectors u_B and v_B are the *u*- and *v*-coordinates of the space boundary. Vertical search interchanges *u* and *v* in the search loop while upward tracking interchanges them in the tracking loop.

spaces. In these sequential computations, the upper boundary of one space is the lower boundary of the subsequent space. Thus, allowing sequential generation of the IGPs of the successive spaces, as their boundaries are constructed. The accuracy of the generated IGPs is verified by monitoring the flip in the sign of the cutoff dispersion function between successive spaces excluding those due to pole crossings. The final outcome is a two-dimensional modal map of selected array parameters, which support different

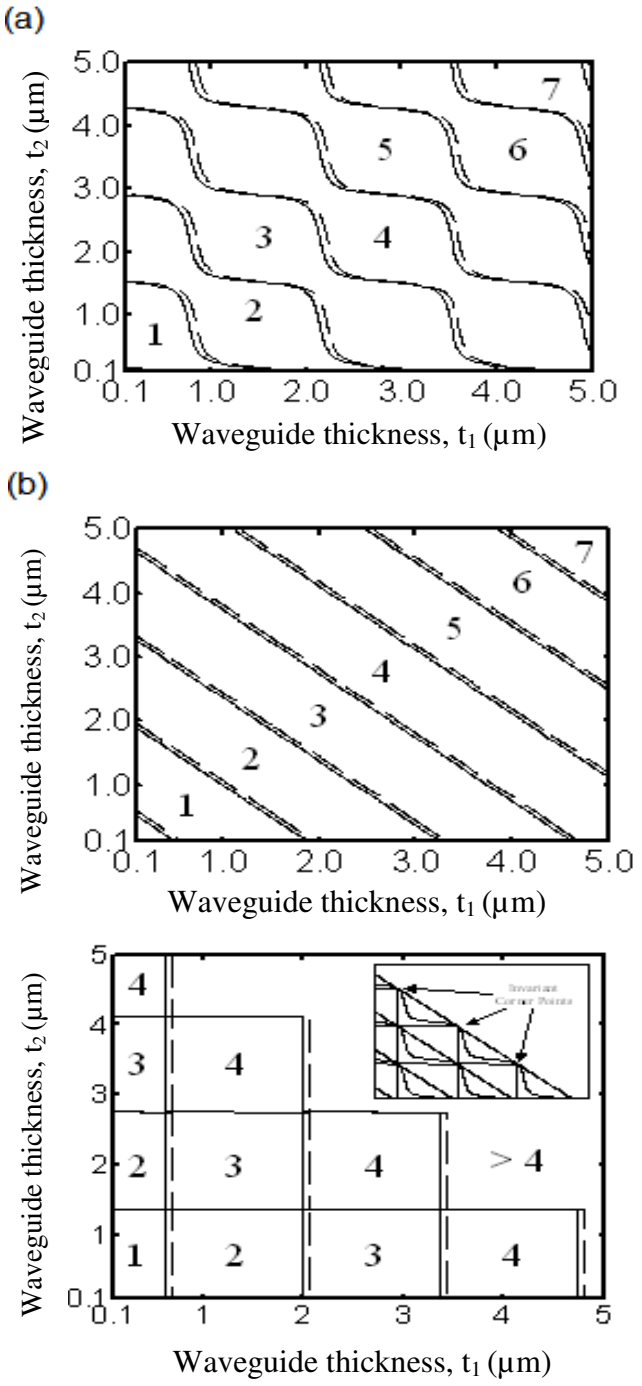

Figure 4. Modal map of TE (solid) and TM (dashed) modes of two coupled waveguides of thickness t_1 and t_2 separated by (a) $s_{1,2}$ = 1 μm, (b) $s_{1,2}$ = 0, and (c) $s_{1,2}$=∞. The upper cladding thickness is h=0 while the refractive indexes are n_1=n_2=3.2, n_a=1, and n_s=3.15. The computations were carried out at λ_o=1.55 μm. The number of modes is indicated in each zone. The size of the zone supporting zero modes is greatest at (b), almost disappears at (a), and completely vanishes at (c). The inset shows the evolution of the boundaries with increasing separation. It shows the corner boundary points which have fixed positions during this evolution.

number of modes.

Limitations on thickness

Uniformity in waveguide refractive index

As an example to illustrate the utility of the proposed algorithm, it is applied to an array of two coupled waveguides, which is commonly used in many photonic devices, e.g. in (Raburn et al., 2000; Lee et al., 2004; Hammer et al., 2004; Passaro and Masanovic, 2006; Saeedkia and Safavi-Naeini, 2007). The thickness, t_1 and t_2, and the separation, $s_{1,2}$, are allowed to change independently keeping other array parameters fixed. These parameters are, n_1 = n_2 = 3.2, n_s = 3.15, n_a = 1, and h = 0. The computations were carried out at $s_{1,2}$ = 1 μm and λ_o=1.55 μm using a MATLAB code that applies the SAT algorithm to the t_1 - t_2 plane (replacing u with t_1 and v with t_2). The algorithm starts with an IGP (t_1 = 0.1 μm, t_2=0.1 μm), which supports zero modes according to the analytical design rules of uniform arrays (Ramadan, 2009). The computational steps along t_1 and t_2 are 10^{-4} μm and 10^{-2} μm, respectively. A vertical search path starting from the IGP was selected with downward staircase tracking. Next, the upper boundaries of the spaces supporting successive number of modes were computed for both TE and TM polarizations. They result in the modal map of Figure 4(a), which shows combinations of t_1 and t_2 (in the range 0.1 μm < t_1,t_2 < 5 μm) supporting one to seven modes. The CPU times (Intel CoreTM 2 Duo Processor T7400 with 2.16 GHz) for these computations are 112.389 s and 89.921 s for the TE and TM modes, respectively.

In order to investigate the effect of coupling on this modal map, two extreme coupling conditions were examined. The first one is the strong coupling limit when $s_{1,2} \to 0$. In this limit, the two waveguides merge to a single asymmetric guide. Its overall thickness for supporting N modes is limited by, $(N-1)\pi + T_a < T_1 + T_2 < N\pi + T_a$, where $T_a = \tan^{-1}(1/\sigma)$ (Adams, 1981). Therefore, the boundaries of the modal map in Figure 4(b) become straight lines. Because of the uniformity of the waveguide refractive index, the magnitude of their slope is unity. The second extreme coupling condition is the weak coupling limit, $s_{1,2} \to \infty$. The corresponding modal map has stair-case boundaries which meet at corner points to form square-shaped zones, as shown in Figure 4(c). As expected, the cutoff conditions of the TE and TM modes only split along the t_1-axis, because of the asymmetry of the surface guide. They coincide with each other along the t_2-axis because of the symmetry of the second isolated waveguide, which is closer to the substrate. This result agrees with the theory of these waveguides (Adams, 1981). The modal map in Figure 4(c) shows that several zones support the same number of array modes. For example, there are four zones which support N = 4 modes. In the weak coupling limit, this number is the same as the overall number of modes supported by the isolated waveguides. Inspection of these four zones shows that they differ in the contribution of each of the two-coupled guides to N. They correspond to the pairs (0, 4), (1, 3), (2, 2) and (3, 1), where the first and second numbers in parenthesis are the numbers N_1 and N_2 (= N-N_1) of the isolated modes supported by the first and second guides of the array, respectively. Similarly, the zones supporting N = 3 arrays modes correspond to (0,3), (1,2), and (2,1). Indeed, N_1 increases with t_1 while N_2 increases with t_2, which allows identifying the zones of these pairs in Figure 4(c). We shall use the notation $N_{N1,N2}$ to distinguish between these zones. For example, the zone $4_{1,3}$ is the zone supporting N=4 with N_1=1, and N_2=3 modes.

Comparing between Figures 4(c) and (a) shows that, as the

separation decreases from infinity to 1μm, the modal map evolve so that part of the $4_{2,2}$ zone (of Figure 4(c) becomes occupied by the $3_{1,2}$ zone (of Figure 4(c)). This occupation indicates that the increase in coupling (with decreasing $s_{1,2}$) reduces the overall number of array modes by one (for the combinations of t_1 and t_2 in the occupied area). Moreover, it shows that the lost mode corresponds to guide 1 (not guide 2), since only N_1 has changed during this decrease in N. Note that under finite (as opposed to infinite) separation of the asynchronous guides, N_1 represents the number of modes which are primarily (as opposed to entirely) localized in guide 1. The oscillatory boundaries of Figure 4(a) may be regarded as an amplitude modulation of the straight-line boundaries in Figure 4(b), which stems from the spatial splitting in the index profile due to separation. It increases with increasing separation. In this sense, the boundaries in Figure 4(c) may be regarded as a stronger amplitude modulation of these straight lines, in which the sinusoidal-like boundaries of Figure 4(a) evolve to staircase boundaries. During the increase in separation, the spatial period of oscillations remains unchanged along the unmodulated straight-line boundaries. It corresponds to the periodic π-change in the normalized thickness of each isolated waveguide along the orthogonal T_1 and T_2 axes (not shown). Therefore, its derivation is straightforward. It is given by, $\lambda_o / \sqrt{2}\left(n_1^2 - n_s^2\right)$, which is independent of separation.

Detailed inspection of Figure 4 shows that the split in the refractive index of the merged guide, as the separation increases, enforces the peaks of the oscillations of the boundaries towards the origin; keeping the unmodulated straight-line boundaries (at $s_{1,2}$= 0) as their upper envelopes. See the inset of Figure 4(c). In addition, the corner points of Figure 4(c) coincide with these envelops. They remain at invariant positions on the boundaries under all coupling conditions. Thus, as the separation increases, the upper straight-line boundary of the merged waveguide which supports N-1 modes gets inside the zone supporting N modes, except at the corner points which remain on the boundaries; as shown in the inset of Figure 4(c). This observation leads to a simple rule to design an array of two coupled waveguides (with $n_1 = n_2$) which supports N modes (at any non-zero separation). The design rule chooses a point on this upper straight-line boundary, excluding the invariant corner points. The normalized thickness of the waveguides along this boundary satisfies the straight line equation,

$$T_1 + T_2 = (N-1)\pi + T_a, \tag{4a}$$

with

$$T_a = \tan^{-1}(1/\sigma), \tag{4b}$$

excluding $T_1 = T_a$ and all the choices of T_2 or $T_1 - T_a$ which are integer multiples of π. These excluded solutions correspond to the corner boundary points. Even solutions which are close to, but not coinciding with, these points should be avoided in practical designs to maximize tolerance and prevent propagation of unwanted modes due to fabrication imperfections. Indeed, (4) does not give all solutions. Other combinations of T_1 and T_2 which do not satisfy (4) may still support N modes. It may give no solution in specific cases. For example, for a symmetric array ($T_a = 0$), (4) gives no solution when N = 1. Also, it gives no valid solution for a symmetric array when N is any odd number and $T_1 = T_2$. In spite of these restrictions, (4) always gives a solution for an arbitrary number of modes provided that asymmetry ($T_a \neq 0$) is used in the design. Further inspection of (4) shows that it imposes no constraint on the separation between the waveguides. It chooses the thickness, $T_1 + T_2$, which equals the cutoff of the N-order mode of the merged guide. This choice means that the merged guide ($s_{1,2} = 0$) is at the "edge" of supporting N modes but is still supporting N-1 modes. According to (4), splitting the merged guide into two isolated guides ($s_{1,2} \neq 0$) directly adds a mode to these N-1 modes.

Nonuniformity in waveguide refractive index

In order to investigate the effect of non-uniformity in the core refractive index, computations were repeated for M = 2 with n_1 = 3.4 (instead of 3.2), keeping all other parameters (including n_2) the same as before. They started from the same IGP and followed a vertical search with downward tracking algorithm. The computational steps along t_1 and t_2 are 10^{-3} and 10^{-2} μm, respectively. Figure 5 shows the computed modal maps at $s_{1,2}$ = 0 and $s_{1,2}$ = 1 μm. The overall CPU times for these maps are 283.018 and 209.343 s, respectively. As expected, the number of zones increases, which gives rise to higher number of supported modes (within the same computational window) due to the increase in n_1. Figure 5(a) shows that the boundaries of the merged guide ($s_{1,2}$= 0) are no longer straight lines, as in Figure 4(b). They are a modulated version of these lines, which result from the step modulation in the core refractive index of the merged waveguide (by the change in n_1). Again, by increasing the separation to $s_{1,2}$ = 1 μm, the same increase in the magnitude of oscillations is observed, which is accompanied by an evolution towards the stair-case shape, as explained before (Figure 5(b)). The increase in the inclination of the boundaries reflects the increase in n_1 (more modes are counted by moving along the t_1-axis, compared to the t_2-axis). The slope of the straight lines which pass through the corner points in this case (not shown) has a constant magnitude of $\sqrt{\left(n_1^2 - n_s^2\right)/\left(n_2^2 - n_s^2\right)}$. The period of oscillation along these lines is given by, $\lambda_o \sqrt{n_1^2 + n_2^2 - 2n_s^2} \Big/ 2\sqrt{\left(n_1^2 - n_s^2\right)\left(n_2^2 - n_s^2\right)}$, which is, again, independent of separation. Because of the absence of an analytical expression of the boundaries of Figure 5(a) (at $s_{1,2}$=0), no design rule similar to (4) is derived when $n_1 \neq n_2$.

Limitations on separation

Uniformity in waveguide refractive index

In order to identify the design zones for supporting different number of modes in the t_m-$s_{m,m+1}$ space (replacing u with t_m and v with $s_{m,m+1}$), we consider two coupled waveguides of uniform refractive index, $n_1 = n_2$ = 3.2. For simplicity, we initially consider the case of uniform waveguide thickness, t_1=t_2 (=t). The other array parameters are n_s =3.15, n_a = 1, h = 0, and $s_{1,2}$ (=s). This array couples between an asymmetric waveguide, which may support no isolated mode, and a symmetric waveguide, which at least supports a single isolated mode. If the uniform thickness of both guides is below the cutoff of the zero-order mode of the asymmetric waveguide, then the array supports a single mode at any separation between the

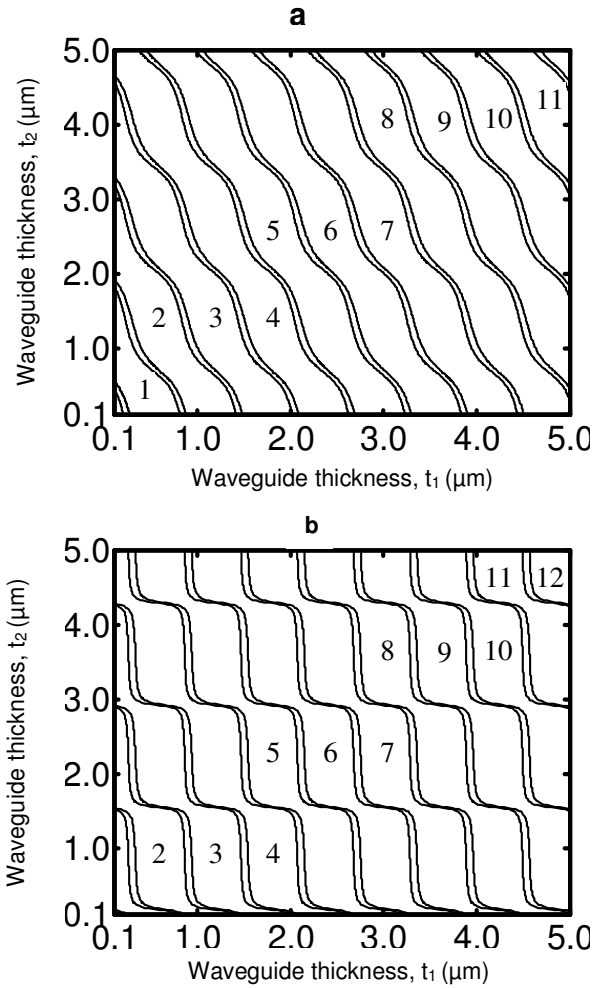

Figure 5. Modal map of TE (solid) and TM (dashed) modes of two coupled waveguides of thickness t_1 and t_2 separated by (a) $s_{1,2}$ =0 and (b) $s_{1,2}$ = 1 μm. The upper cladding thickness is h = 0 while the refractive indexes are n_1=3.4, n_2=3.2, n_a = 1, and n_s=3.15. The computations were carried out at λ_o=1.55 μm. The number of modes is indicated in each zone. The size of the zone supporting zero modes is greatest at (a), almost disappears at (b).

waveguides (up to $s = \infty$). This preliminary analysis indicates that the zone of the *t*-*s* space supporting a single array mode is open (has no maximum separation) along this range of thickness. If vertical search is used by the SAT algorithm to allocate the boundaries of this zone, it may lead to infinite search loops. To avoid this run-time error, we use a horizontal search with downward tracking algorithm to allocate the boundaries of the zones of this array in the *t*-*s* plane. The algorithm starts with an IGP (t = 0.001 μm and s =5 μm) and follows the sequential approach described above (in Section 4.1) to generate the other IGPs, which reconstructs the different zone boundaries. The computational steps along t and s are 10^{-3} μm and 10^{-2} μm, respectively. The results are shown in Figure 6(a) for both TE and TM modes. The overall CPU time for these computations is 135.702 s. The points of intersection of these boundaries with the *t*-axis correspond to the solutions depicted by (4). For example, substituting with N = 1 and $T_1 = T_2 (= T)$ into (4), results in $T = T_a/2$, which gives t = 0.30 μm and t = 0.34 $\mu\mu$ for TE and TM modes, respectively. If we start moving from the intersection point (t = 0.30 μm, s = 0), or (t = 0.34 μm, s = 0), in the vertical direction (of increasing s) then the number of supported modes of the specific polarization becomes N = 1 (instead of N=0 at the starting point). This motion is equivalent to splitting the merged guide (s = 0), by arbitrary separation ($s \neq 0$), to support N (instead of N - 1) modes. It is clear from Figure 6(a) that the intersection points are not the only points satisfying these coupling-independent designs. They are satisfied by a range of t extending from each intersection point, which may be used to improve the tolerance of these designs. To support a single mode (N = 1), independent of coupling, for both modal polarizations, the thickness t must be greater than or equal to 0.34 μm of the TM polarization and at the same time belongs to this range, e.g. t = 0.5μm. Thus, to have the same number of modes of both polarizations it is sufficient to solve (4) for the TM modes (because of the larger cutoff of the TM modes). It may also be noted that the same coupling-independent properties of the N=1 zone apply to all other zones (supporting different N). This note confirms the ability of (4) to provide a solution of T_1 and T_2 for any arbitrary N in the case of asymmetric arrays.

The effect of nonuniformity in the thickness of the isolated waveguides was investigated by imposing the condition, $t_1 = 2t_2$ (instead of t_1=t_2) on the previous array and repeating computations. The results are shown in Figure 6(b), which plots the modal map of the TE modes in the t_1-s plane. Again the boundary points at s = 0 are solutions of (4) which support the required number of modes at any separation. For example, for N = 1, the merged waveguide point (t_1 = 0.4 μm and s = 0) corresponds to the solution, $T_1 + T_2 = 1.5T_1 = T_a$. For N = 2, the point (t_1 = 1.32 μm and s = 0) corresponds to the solution, $1.5T_1 = \pi + T_a$, and so on. To examine the limitations on the generalization of (4) to higher M, we consider an array of three waveguides with uniform thickness t and uniform core refractive index (n_1 = n_2 =n_3 = 3.2), keeping all other parameters the same as before. The results of computations are shown in Figure 6(c) for the TE modes. According to this, Figure 4 may be generalized by replacing $T_1 + T_2$ with $3T$ only if N is an integer multiple of M (e.g. N = 3 and N = 6).

Nonuniformity in waveguide refractive index

If nonuniformity is introduced by using n_1 = 3.4 (instead of 3.2) in the array of two coupled waveguides of the previous section (with t_1 = t_2), then the SAT algorithm reveals the modal map of Figure 7(a). It is a modified version of Figure 6(a) which results from the modification of n_1. As expected, the modal cutoffs are modified, theperiodicity of the map is smeared and the number of supported modes is higher for the same computational window. Also, the tolerance in t of the coupling-independent designs in some zones almost vanishes. For example, as in the zones supporting N = 1 and N = 4 modes. The small offset between the cutoff of the TE and TM modes of the latter zone (N = 4) eliminates the overlap between their infinitesimally small coupling-independent ranges on the *t*-axis. This elimination means that it is impossible to have a coupling-independent design of the specific array, which simultaneously supports four modes of both TE and TM polarizations. In spite of these results, the tolerance of the coupling-independent designs of other zones is comparable to the case of uniform refractive index of Figure 6(a), e.g. at N = 2, 3 and 6. The results of applying the SAT algorithm to an array of three waveguides of uniform thickness and

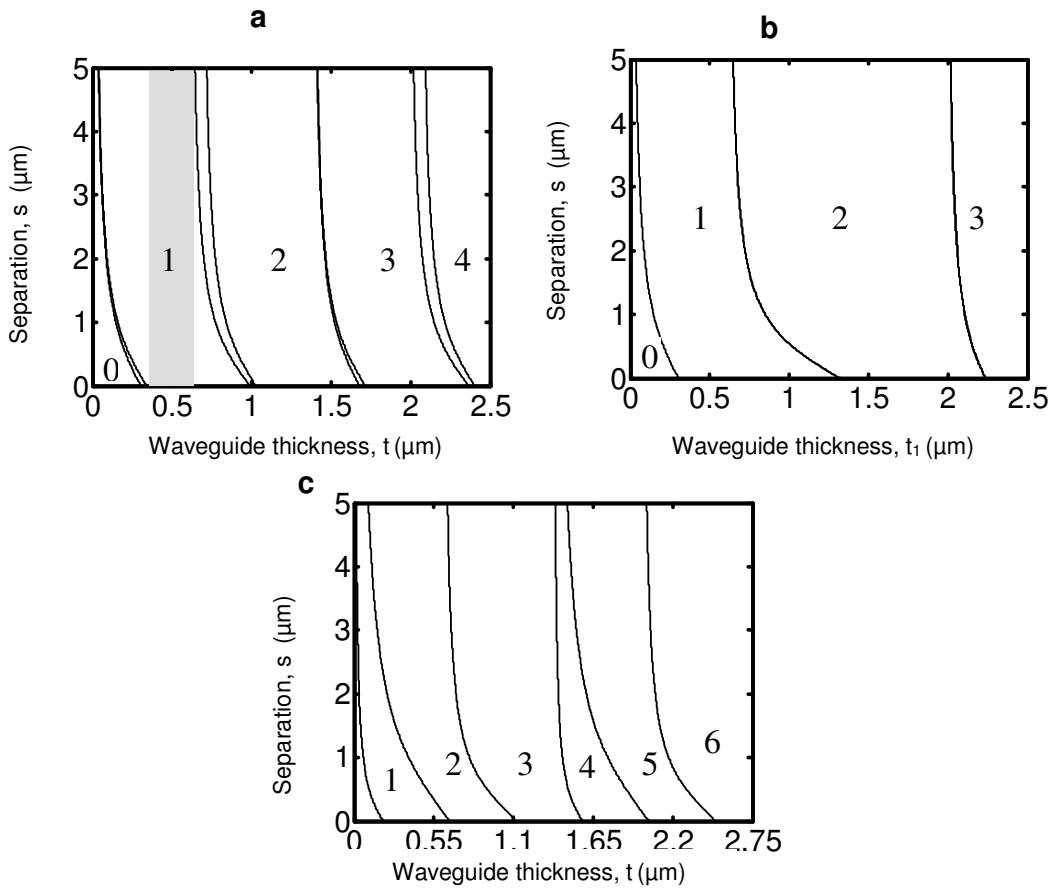

Figure 6. Modal map of TE (solid) and TM (dashed) modes of arrays of waveguides with uniform core refractive index of 3.2 and separation *s* when (a) *M=2*, $t_1=t_2(=t)$, (b) *M=2*, $t_1=2t_2$, and (c) *M=3*, $t_1=t_2(=t)$. The computations were carried out at λ_o=1.55 μm, h = 0, n_a=1, and n_s=3.15. The number of modes is indicated on each zone. The shading in (a) defines the open coupling-independent region supporting a single mode for both TE and TM polarizations. The leftmost zone in (c) supports zero modes.

nonuniform waveguide refractive index (n_1 = 3.4, n_2 = 3.3, and n_3 = 3.2) are shown in the TE modal map of Figure 7(b). In spite of the small increase in *M*, the boundaries of some of the zones become much more closer to each other. See the zones supporting 2, 4 and 6 TE modes. They almost coincide for the latter zone (N = 6). This closeness of boundaries, as *M* increases, requires careful selection of the numerical parameters of the algorithm to resolve the small differences in *t* between them.

DISCUSSION

While the examples presented above have no specific device application, they may directly be extended to the design and optimization of different photonic devices. For example, the design of the spot sizes converter (SSC) in (Buus et al., 1993), which matches between the modes of a semiconductor laser and a single-mode fiber. This converter consists of an array of three vertically coupled waveguides, which support three modes. Its modal-expansion mechanism is based on interference between the zero-order and the second-order array modes. A precise alignment of the launched modal field with the central waveguide of the SSC prevents excitation of the first-order array mode. The thickness of the guides and their separation are allowed to vary keeping $t_1 = t_3$ and $s_{1,2} = s_{2,3}(=s)$ to ensure symmetric modal profiles. It is analyzed in Buus et al. (1993) using coupled mode theory. An alternative approach, which is not restricted by the weak coupling approximation, is to use the SAT algorithm to identify the s-t_1 space which supports three array modes (N = 3) at different ratios of t_2/t_1 in exactly the same way as described in previous examples. This approach identifies the design parameter space that covers both weak and strong coupling conditions. The absence of approximations in the SAT algorithm (compared to coupled mode theory) allows exploiting all the degrees of freedom in the design of the SSC. Computations of the coupling efficiency from laser to fiber

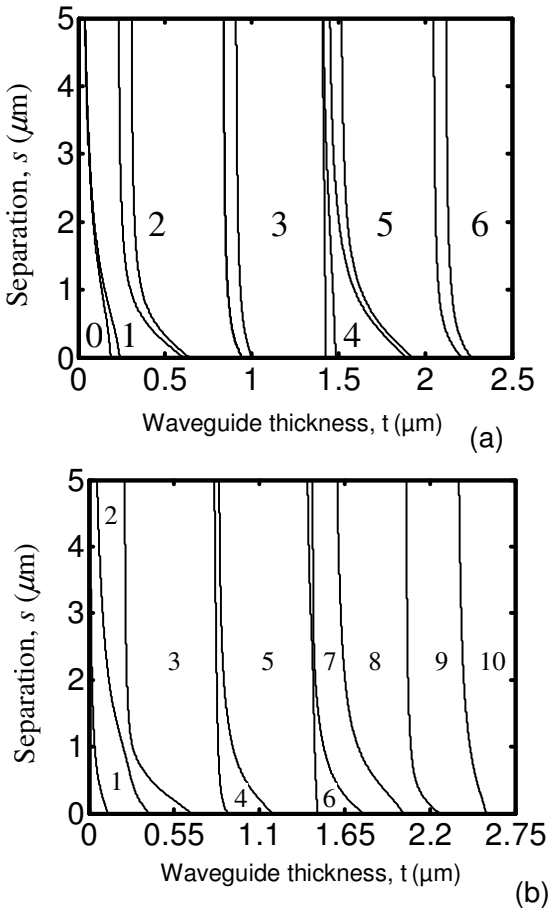

Figure 7. Modal map of TE (solid) and TM (dashed) modes of arrays of waveguides with nonuniform core refractive index, uniform waveguide thickness *t,* and separation *s*, when (a) *M=2*, n_1*=3.4*, and n_3 =3.2 (b) *M=3*, n_1*=3.4,* n_2=3.3 and n_3=3.2. The computations were carried out at λ_o=1.55 μm, *h* = 0, n_a=1, and n_s=3.15. The number of modes is indicated on each zone. The leftmost zone supports zero modes.

may then proceed in the same way as in Buus et al. (1993) over a wider parameter space for ultimate improvement of the SSC performance. The conversion of the vertical array design to a strip-loaded geometry may be done using the effective index approximation (Adams, 1981). In this case, the requirement of a single lateral mode supported by the strip-loaded guide must be satisfied by all three modes. A similar application of the effective index method has been used in rib-like waveguide supporting three guided modes in the vertical direction (Buckman, 1983).

Conclusion

A numerical algorithm has been proposed for the design of both uniform and nonuniform arrays of optical waveguides. It identifies the array parameters, which support different number of modes. This identification is of great importance in the absence of analytical design rules, specifically for nonuniform arrays. It is a key step in designing guided-wave devices, which allows optimizing their performance over well-defined parameter spaces. The algorithm studied the effect of changing the waveguide thickness, refractive index, and separation on the number of guided modes of arrays of two coupled waveguides. The analysis of the results lead to the deduction of a simple straight-line design rule, which allows controlling of the number of modes of these arrays by controlling their nonuniform waveguide thickness provided that they have uniform core refractive index. The rule may particularly be useful if the thickness of one of the waveguides is limited by some design constraints and it is required to maintain a constant number of modes supported by the coupled waveguide system. In this case, it directly gives a feasible range of thickness for the other waveguide, which may be used as a starting range for further detailed analysis done by the algorithm itself or by another numerical tool. It has been shown that generalization of the design rule to arrays supporting larger number of waveguides is only possible for specific number of modes. The effect of gain or loss in array guides on the feasible design parameters identified by the algorithm may be investigated using other numerical tools, e.g. in (Schlereth and Tacke, 1990; Scarmozzino et al., 2000). The algorithm was also applied to arrays of three waveguide. It has been shown that as the number of waveguides increases the modal map becomes crowded with different zones and sensitive to numerical errors, even at small number of waveguides. These changes in the modal map are stronger for arrays with nonuniform waveguide refractive index, which require higher resolution and careful selection of the numerical parameters.

REFERENCES

Adams MJ (1981). An Introduction to Optical Waveguides. New York: Wiley.

Belabas N, Bouchoule S, Sagnes I, Levenson JA, Minot C, Moison JM (2009). Confining light flow in weakly coupled waveguide arrays by structuring the coupling constant: towards discrete diffractive optics. Opt. Express, 17: 3148-3156.

Buckman AB (1983). Mode selection with a three-layer dielectric rib waveguide. J. Opt. Soc. Amer., 73: 33-36.

Buus J, Stewart WJ, Haes J, Willems J, Baets RG (1993). Spot size expansion for laser-to-fiber coupling using an integrated multimode coupler. J. Lightw. Technol., 11: 582-588.

Chiang KS (1991). Effective-index method for the analysis of optical waveguide couplers and arrays: An asymptotic theory. J. Lightw. Technol., 9: 62-72.

Chiang KS (1992). Coupled-zigzag-wave theory for guided waves in slab waveguide arrays. J. Lightw. Technol., 10: 1380-1387.

Dross F, van Dijk F, Parillaud O, Vinter B, Vodjdani N. (2005). Single-transverse-mode InGaAsP-InP edge-emitting bipolar cascade laser.

IEEE J. Quantum Electron., 41: 1356-1360.
Hammer JM, Evans GA, Ozgur G, Butler JK (2004). Isolators, polarizers, and other optical waveguide devices using a resonant-layer effect. J. Lightw. Technol. 22: 1754–1763.
Hardy A, Marom E, Shama Y (1988). Power transfer in asymmetric multiport couplers. Appl. Opt., 27: 447-448.
Hardy A, Streifer W (1986). Coupled modes of multiwaveguide systems and phased arrays. J. Lightw. Technol., LT-4: 90-99.
Hardy A, Streifer W, Osinski M (1986). Coupled-mode equations for multimode waveguide systems in isotropic or anisotropic media. Opt. Lett., 11: 742-744.
Kawakita Y, Saitoh T, Shimotaya S, Shimomura K (2004). A novel straight arrayed waveguide grating with linearly varying refractive-index distribution. IEEE Photon. Technol. Lett., 16: 144-146.
Lee Y, Mishima T, Kominami S, Shinoda K, Uchiyama H (2004). Dispersion compensation by two vertically coupled asymmetric ridge waveguides. Appl. Opt., 43: 4101-4105.
Liu ZS, Magnusson R (2002). Concept of multiorder multimode resonant optical filters. IEEE Photon. Technol. Lett. 14: 1091-1093.
Marcuse D (1987). Bandwidth of forward and backward coupling directional couplers. J. Lightw. Technol., LT-5: 1773–1777.
Menon VM, Xia F, Forrest SR (2005). Photonic integration using asymmetric twin-waveguide (ATG) technology: Part II-Devices. IEEE
J. Sel. Topics Quantum Electron, 11: 30-42.
Passaro VMN, Masanovic GZ (2006). Design of SiON-based grating-assisted vertical directional couplers. Opt. Express, 14: 1055-1063.
Raburn M, Liu B, Abraham P, Bowers J (2000). Double-bonded InP-InGaAsP vertical coupler 1:8 beam splitter. IEEE Photon. Technol. Lett., 12: 1639-1641.
Rajarajan M, Rahman BMA, Grattan KTV (2003). A novel and compact optical polarizer incorporating a layered waveguide core structure. J. Lightw. Technol., 21: 3463-3470.
Ramadan TA (2008). A recurrence technique for computing the effective indexes of the guided modes of coupled single-mode waveguides. Progress In Electromagnetics Research M, 4: 33-46.
Ramadan TA (2009). Sturm-sequence properties of recurrence dispersion functions of periodic waveguide arrays: Theory and applications. J. Lightw. Technol., 27: 4548-4562.
Ramadan TA, Scarmozzino R, Osgood RM Jr. (2000). A novel 1x4 coupler-multiplexer permutation switch for WDM applications. J. Lightw. Technol., 18: 579-588.
Ruschin S, Griffel G, Hardy A, Croitoru N (1986). Unified approach for calculating the number of confined modes in multilayered waveguiding structures. J. Opt. Soc. Amer. A, 3: 116-123.
Saeedkia D, Safavi-Naeini S (2007). Modeling and analysis of a multilayer dielectric slab waveguide with applications in edge-coupled terahertz photomixer sources. J. Lightw. Technol., 25: 432-439.
Scarmozzino R, Gopinath A, Pregla R, Helfert S (2000). Numerical techniques for modeling guided-wave photonic devices. IEEE J. Sel. Topics Quantum Electron. 6: 150-162.
Schlereth KH, Tacke M (1990). The complex propagation constant of multilayer waveguides: An algorithm for a personal computer. IEEE J. Quantum Electron. 26: 627-630.
Shama Y, Hardy AA, Marom E (1989). Multimode coupling of unidentical waveguides. J. Lightw. Technol. 7: 420-425.
Syms RRA (1987). Approximate solution of eigenmode problems for layered coupled waveguide arrays. IEEE J. Quantum Electron. QE-23: 525-532.
Xia F, Menon VM, Forrest SR (2005). Photonic integration using asymmetric twin-waveguide (ATG) technology: Part I-Concepts and theory. IEEE J. Sel. Topics Quantum Electron, 11: 17-29.
Zhao AP, Cvetkovic SR, Punjani M (1992). Analysis of stripe multilayer waveguides with effective index and finite element methods. IEEE J. Quantum Electron, 28: 573-579.

APPENIDX A: POLES OF THE DISPERSION FUNCTION

The dispersion function of the coupled waveguide array described in the background theory is derived in terms of the normalized propagation constant, $b=(\delta_e-1)/(\delta_f-1)$, following the approach in (Chiang, 1992) and (Ramadan, 2008). Here, $\delta_e=n_e^2/n_s^2$, and $\delta_f=\max_m \delta_m$, which limits *b* between zero and unity. The derived dispersion function has two groups of poles. The poles of the first group are given by,

$$b_m^{(1)}=(\delta_m-1)/(\delta_f-1). \quad \text{(A1)}$$

Each waveguide generates one of these poles. They never cross the cutoff point (*b*=0) due to changing any of the waveguide parameters. The poles of the second group are given by,

$$b_{m,p}^{(2)}=b_m^{(1)}\left(1-p^2\pi^2/T_m^2\right), \quad \text{(A2)}$$

where *p* = 1, 2,..,$\lfloor T_m/\pi \rfloor$, for each waveguide of $T_m \geq \pi$. Here, $\lfloor z \rfloor$ denotes the floor of *z*. One of these poles crosses the cutoff point each time T_m becomes an integer multiple of π along a search path.

APPENIDX B: PROOF OF THE CHANGE IN THE SIGN OF C_M WITH THE CROSSING OF A SINGLE POLE

To investigate the effect of the crossing of a pole on the sign of C_M, it is expressed as a determinant of a tri-diagonal matrix,

$$C_M=\det\begin{pmatrix} \rho_M & \kappa_M & & & & \\ 1 & \rho_{M-1} & \kappa_{M-1} & & & \\ & 1 & \rho_{M-2} & \kappa_{M-2} & & \\ & & \bullet & \bullet & \bullet & \\ & & & 1 & \rho_{m+2} & \kappa_{m+2} \\ & & & & 1 & C_{m+1} \end{pmatrix}, \quad \text{(B1)}$$

where, C_{m+1} is the cutoff dispersion function for the first *m*+1 waveguides of the array. Next, the normalized thickness of a the m^{th} array guide, T_m, is expressed as, $T_m=q\pi\pm\Delta$, in the vicinity of $q\pi$, where Δ is infinite-simally small. Out of the matrix elements in (B1), only C_{m+1} depends on T_m. It depends on it through the dependence of the three recurrence parameters, ρ_m, ρ_{m+1}, and κ_{m+1} on T_m. The $\cot(T_m)$ and $\sec^2(T_m)$ terms in these parameters (see (2)) become infinitely high when Δ tends to zero. Therefore, with the assumption that no other normalized thickness is an integer multiple of π, these terms dominate over other terms, which results in, $\rho_m=\pm 1/\Delta$, $\rho_{m+1}=\pm\eta_{m,m+1}/\Delta$, and $\kappa_{m+1}=\eta_{m,m+1}/\Delta^2$, where we have used $\cos(\Delta)\approx 1$ and $\sin(\Delta)\approx\Delta$. These approximations become exact in the limit when $\Delta\to 0$. Now, $C_{m+1}=(\pm\eta_{m,m+1}/\Delta)C_m-(\eta_{m,m+1}/\Delta^2)C_{m-1}$ while $C_m=(\pm 1/\Delta)C_{m-1}-\kappa_m C_{m-2}$. Therefore, $C_{m+1}=(\mp\eta_{m,m+1}\kappa_m/\Delta)C_{m-2}$, which changes its sign when T_m crosses $q\pi$. Next, filtering out C_{m+1} from the determinant of (B1) allows writing C_M as the product of C_{m+1} and the matrix,

$$U_M^m=\det\begin{pmatrix} \rho_M & \kappa_M & & & & \\ 1 & \rho_{M-1} & \kappa_{M-1} & & & \\ & 1 & \rho_{M-2} & \kappa_{M-2} & & \\ & & \bullet & \bullet & \bullet & \\ & & & 1 & \rho_{m+2} & \end{pmatrix}, \quad \text{(B2)}$$

where we have used $1/C_{m+1}=(\mp\Delta/\eta_{m,m+1}\kappa_m)(1/C_{m-2})\to 0$ as $\Delta\to 0$. Since U_M^m is independent of T_m, the limit, $\lim_{\Delta\to 0}C_M=(\lim_{\Delta\to 0}C_{m+1})(\lim_{\Delta\to 0}U_M^m)=\pm\infty$, which proves that C_M must change its sign when T_m crosses $q\pi$. This result concludes the proof.